BJR

https://doi.org/10.1259/bjr.20220068

Received: 13 January 2022 | Revised: 07 November 2022 | Accepted: 20 November 2022 | Published online: 12 January 2023

Cite this article as:
Lin F, Li Q, Wang Z, Shi Y, Ma H, Zhang H, et al. Intratumoral and peritumoral radiomics for preoperatively predicting the axillary non-sentinel lymph node metastasis in breast cancer on the basis of contrast-enhanced mammography: a multicenter study. *Br J Radiol* (2023) 10.1259/bjr.20220068.

FULL PAPER

Intratumoral and peritumoral radiomics for preoperatively predicting the axillary non-sentinel lymph node metastasis in breast cancer on the basis of contrast-enhanced mammography: a multicenter study

[1]FAN LIN, MD, [2]QIN LI, MD, PhD, [1]ZHONGYI WANG, MD, [1]YINGHONG SHI, MD, PhD, [1]HENG MA, MD, PhD, [3]HAICHENG ZHANG, MSc, [4]KUN ZHANG, MD, PhD, [5]PING YANG, MD, PhD, [6]RAN ZHANG, MD, [7]SHAOFENG DUAN, MD, PhD, [8]YAJIA GU, MD, PhD, [1,3]NING MAO, MD, PhD and [1]HAIZHU XIE, MD, PhD

[1]Department of Radiology, Yantai Yuhuangding Hospital, Affiliated Hospital of Qingdao University, Yantai, China
[2]Department of Radiology, WeiFang Traditional Chinese Hospital, Weifang, China
[3]Big Data and Artificial Intelligence Laboratory, Yantai Yuhuangding Hospital, Affiliated Hospital of Qingdao University, Yantai, China
[4]Department of Breast Surgery, Yantai Yuhuangding Hospital, Affiliated Hospital of Qingdao University, Yantai, China
[5]Department of Pathology, Yantai Yuhuangding Hospital, Affiliated Hospital of Qingdao University, Yantai, China
[6]Huiying Medical Technology, Beijing, China
[7]GE Healthcare, Shanghai, China
[8]Department of Radiology, Fudan University Shanghai Cancer Center, Shanghai, China

Address correspondence to:
Dr Haizhu Xie
E-mail: *xhz000417@sina.com*
Ning Mao
E-mail: *maoning@pku.edu.cn*

The authors Fan Lin and Qin Li contributed equally to the work.

Objective: To develop and test a contrast-enhanced mammography (CEM)-based radiomics model using intratumoral and peritumoral regions to predict non-sentinel lymph node (NSLN) metastasis in breast cancer before surgery.
Methods: This multicenter study included 365 breast cancer patients with sentinel lymph node metastasis. Intratumoral regions of interest (ROIs) were manually delineated, and peritumoral ROIs (5 and 10 mm) were automatically obtained. Five models, including intratumoral model, peritumoral (5 and 10 mm) models, and intratumoral+peritumoral (5 and 10 mm) models, were constructed by support vector machine classifier on the basis of optimal features selected by variance threshold, SelectKbest, and least absolute shrinkage and selection operator algorithms. The predictive performance of radiomics models was evaluated by receiver operating characteristic curves. An external testing set was used to test the model. The Memorial Sloan Kettering Cancer Center (MSKCC) model was used to compare the predictive performance with radiomics model.
Results: The intratumoral ROI and intratumoral+peritumoral 10-mm ROI-based radiomics model achieved the best performance with an area under the curve (AUC) of 0.8000 (95% confidence interval [CI]: 0.6871–0.8266) in the internal testing set. In the external testing set, the AUC of radiomics model was 0.7567 (95% CI: 0.6717–0.8678), higher than that of MSKCC model (AUC = 0.6681, 95% CI: 0.5148–0.8213) (p = 0.361).
Conclusions: The intratumoral and peritumoral radiomics based on CEM had an acceptable predictive performance in predicting NSLN metastasis in breast cancer, which could be seen as a supplementary predicting tool to help clinicians make appropriate surgical plans.
Advances in knowledge: The intratumoral and peritumoral CEM-based radiomics model could noninvasively predict NSLN metastasis in breast cancer patients before surgery.

INTRODUCTION

Breast cancer is one of the most common malignancies in females worldwide and one of the main causes of cancer deaths.[1] The status of axillary lymph node (ALN) metastasis is not only an important independent factor affecting the prognosis of breast cancer patients,[2] but also an important

clinical indicator that guides the choice of adjuvant therapy. Axillary lymph node dissection (ALND) is the most accurate method to evaluate the status of ALN in breast cancer, but it can easily cause lymphatic and venous return disorders and even nerve damage.[3–5] Study has shown that about two-thirds of patients who underwent ALND have no metastasis in the non-sentinel lymph node (NSLN) among patients with one or two positive sentinel lymph nodes (SLNs).[6]

The results of the American College of Surgical Oncology Group (ACOSOG) Z0011 trial and the International Breast Cancer Study Group (IBCSG) 23–01 trial showed that there was no significant difference in the efficacy of further axillary radiotherapy and ALND for breast cancer patients.[7,8] Although these trials provided evidence for reducing unnecessary ALND, they had certain applicable conditions, such as early breast cancer (cT1-2N0M0), patients with 1–2 positive SLNs, receiving breast conserving surgery, and tumor less than 5 cm in diameter. Breast cancer patients who did not meet the eligibility criteria still received ALND routinely. In clinical practice, accurately predicting the risk of non-sentinel lymph node metastasis in patients with positive SLNs will help clinicians to select high-risk patients for ALND and exempt low-risk patients from ALND. Therefore, clarifying whether breast cancer patients have NSLN metastasis is of great clinical significance.

Many institutions have proposed NSLN metastasis predictive models. The Memorial Sloan Kettering Cancer Center (MSKCC) model is the most widely validated model to predict NSLN metastasis in the world. However, its validation results varied greatly among different populations, with the area under the curves (AUCs) ranging from 0.53 to 0.86.[9–11] Bi et al[12] and Liu et al[13] had verified the predictive value of the MSKCC model in Chinese breast cancer patients, yielding AUCs of only 0.722 and 0.624, respectively, indicating that a more accurate NSLN metastasis predictive tool is needed.

Lambin et al first proposed the concept of radiomics in 2012.[14] Compared with traditional imaging findings, such as shape, size, margins, internal enhancement pattern, etc., radiomics can deeply mine features from medical images that are invisible to the human eyes.[15] To some extent, radiomics features can help assess tumor heterogeneity, and radiomics models can be established to assist decision-making. Studies have shown that intratumoral-based radiomics has good performance in classifying breast lesions and predicting the efficacy of neoadjuvant chemotherapy and lymph node metastasis in breast cancer patients.[16–19] Others studies have shown that the peritumoral-based radiomics may provide additional value in predicting ALN metastasis and pathological complete response to neoadjuvant chemotherapy in breast cancer.[20–22] The performance of radiomics combined with intratumoral and peritumoral regions in predicting NSLN metastasis in breast cancer patients has not been fully reported.

Contrast-enhanced mammography (CEM) is a newly emerging breast imaging technology in recent years, which combines intravenous iodine contrast agent and mammography. CEM can not only reflect the glandular structure and calcification of the breast, but also reflect its blood supply through the enhancement degree of the lesion. Studies have shown that CEM has similar sensitivity and positive predictive value to magnetic resonance imaging (MRI) in detecting lesions.[23] Our previous research[24] showed that CEM-based radiomics had good predictive performance in predicting ALN metastasis, but its performance in predicting NSLN metastasis was still unclear.

The purpose of this study is to extract intratumoral and peritumoral radiomics features from the preoperative CEM images of breast cancer patients, and establish a radiomics model to predict NSLN metastasis.

METHODS AND MATERIALS

Patients and sets

The training and internal testing sets in this retrospective study were collected from Center one from July 2017 to June 2020, while the external testing set was collected from Center two from March 2016 to February 2020. This study was approved by the institutional ethics committee of both hospitals, and patients' informed consents were waived. The inclusion criteria were as follows: (a) breast cancer patients who received SLN biopsy and ALND, and diagnosed with a complete pathology result, (b) patients who did not receive any preoperative therapy, (c) surgery within 14 days after CEM examination, and (d) patients with complete clinical information. The exclusion criteria were as follows: (a) multifocal or bilateral breast cancer, (b) non-mass lesions without delineate boundaries, (c) biopsy before CEM examination, (d) patients with distant metastasis or other malignancies previously, and (e) patients with poor image quality.

Finally, a total of 365 women (mean age = 55.01±10.34 years; range = 27–80 years) with ALN metastasis were included in this retrospective study, including 194 patients with NSLN metastasis and 140 patients without NSLN metastasis (Figure 1). All patients from Center one were randomly divided into a training set with 220 patients and an internal testing set with 96 patients with a ratio of 7:3. The 49 patients from Center two were enrolled in the external testing set.

CEM examination

All CEM images from center one were obtained with a full-digital breast machine (Senographe Essential, GE Healthcare), while CEM images from center two were obtained with a full-digital breast machine (Senographe Pristina, GE Healthcare). The imaging process of both centers was consistent. The Omnipaque 300 (GE Healthcare, Inc., Princeton, NJ) was used as contrast agent, which was injected into the upper arm vein at a dose of 1.5 ml/kg and injection flow rate of 3.0 ml s^{-1}. Two minutes after injecting the contrast agent, low- and high-energy images were obtained on both cranial caudal (CC) view and mediolateral oblique (MLO) view within 5 min on bilateral breast. To increase the contrast uptake of the lesion, the breast without a suspected lesion was imaged first, and then the images of breast with the suspected lesion were taken. Recombined images were generated through post-processing system.

Figure 1. Flow chart of patients' enrollment.

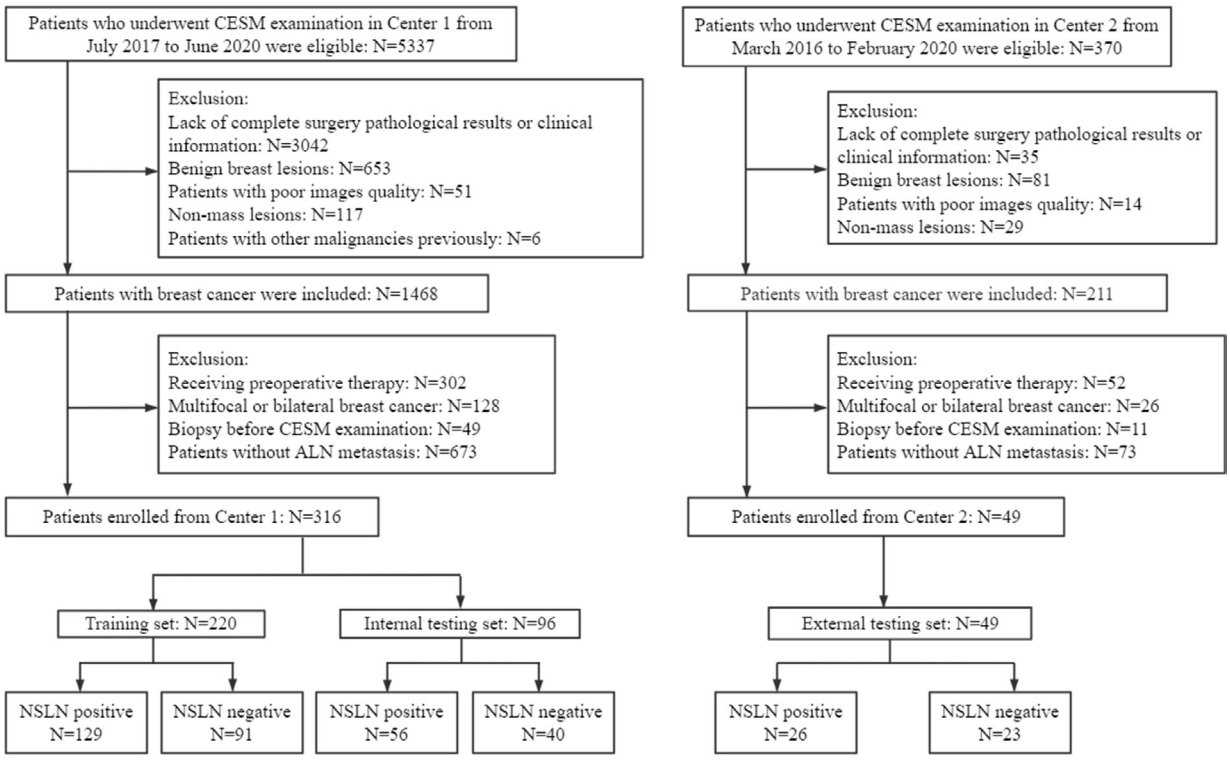

Clinical and radiological characteristics

The status of NSLN metastasis, estrogen receptor (ER), progesterone receptor (PR), human epidermal growth factor receptor Type 2 (HER2), Ki-67, molecular subtypes, lymphovascular invasion, menstrual status and age were obtained from pathological examination results and the medical record system. The diameter of breast cancer was detected on the recombined image on CC view.

Considering that background parenchymal enhancement (BPE) and breast density may be the risk factors of breast cancer,[25,26] BPE was evaluated on MLO view of recombined images in bilateral breast according to enhancement range, while breast density was evaluated on MLO view of low-energy images in bilateral breast according to the amount of fibroglandular tissue.[27] Reader 1 and reader 2 (who had 6 and 11 years' experience in breast imaging, respectively) evaluated the BPE and breast density. If contradictory, the categories of BPE and density were determined by both readers after discussion.

Image segmentation and radiomics feature extraction

All CEM images were downloaded in Digital Imaging and Communications in Medicine (DICOM) format from Picture Archiving and Communication System (PACS). The intratumoral regions of interest (ROIs) were drawn manually on low-energy and recombined images on CC view on ITK-SNAP software (version 3.8.0) by reader 1, who was blinded to the pathology results. Peritumoral ROIs were obtained automatically by uniformly extending the intratumoral ROIs by 5 and 10 mm using the "matplotlib", "SimpleITK", and "radiomics. featureextractor" function packages in Python software (version 3.6). If the peritumoral regions were beyond the parenchyma of the breast after extension, the portion beyond the parenchyma was manually removed. A schematic of ROI segmentation is shown in Figure 2. Finally, five ROIs were generated on each image, including intratumoral ROI (I), peritumoral 5 and 10 mm ROIs (P5, P10), intratumoral+peritumoral 5 and 10 mm ROIs (*I* + P5, *I* + P10).

Image preprocessing was conducted before radiomics feature extraction, including the standardization of the gray value of ROI, gray level discretization, and image resampling by

Figure 2. Examples of ROI segmentation on CEM images. The green region represents the intratumoral region. The yellow region represents the peritumoral 5 mm region. The yellow+blue regions represent the peritumoral 10 mm ROI. The green+yellow regions represent the intratumoral+peritumoral 5 mm ROI. The green+yellow+ blue regions represent the intratumoral+peritumoral 10 mm ROI. (a, c) Low-energy images on CC view. (b, d) Recombined images on CC view.

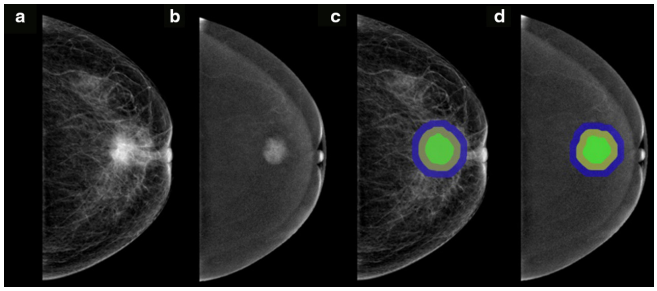

standardizing the images. Quantitative radiomics features were extracted from each ROI using the "RadiomicsFeatureExtractor" package of Pyradiomics, including first-order statistical features, shape-based features, and texture features.

Interobserver and intraobserver agreement of ROI segmentation and feature extraction

The CEM images of 30 patients were randomly selected to evaluate inter- and intraobserver agreement. To evaluate interobserver agreement, reader one repeated the intratumoral ROI segmentation after 3 months. To evaluate intraobserver agreement, reader two used the same method to delineate intratumoral ROIs. The Dice coefficient was used to evaluate the agreement of ROI segmentation, with 0 meaning no overlap and one representing complete consistency. Inter- and intracoefficients (ICCs) were used to assess the reproducibility of radiomics feature extraction. ICCs greater than 0.75 were considered as good agreements.

Radiomics feature selection

The variance threshold, SelectKbest, and least absolute shrinkage and selection operator (LASSO) methods were used in sequence to reduce the redundant features and select optimal radiomics features. The eigenvalues of the variance<0.8 in the variance threshold method and the features with $p < 0.05$ in the SelectKbest method were included. The score function of SelectKbest method was the *mutual_info_regression*. For the LASSO algorithm, the optimal LASSO α parameter was set by five-fold cross-validation, and radiomics features with non-zero coefficients were finally selected in the training set.

Development and validation of the radiomics model

On the basis of the selected features from five ROIs (I, P5, P10, *I* + P5, *I* + P10), five radiomics models were built by support vector machine (SVM) classifier, including intratumoral model (Model 1), peritumoral 5 and 10 mm models (Models 2 and 3), and intratumoral+peritumoral 5 and 10 mm models (Models 4 and 5). Receiver operating characteristic (ROC) curves were drawn to evaluate the predictive performance of radiomics models. In particular, a new radiomics model (Model 6) was developed by SVM through combining features from two ROIs with the highest AUCs in the internal testing set. Moreover, we re-performed feature selection using the same method on the raw extracted radiomics features of the two models with the best AUCs in Models 1–5. Another radiomics model (Model 7) was constructed using the boosting algorithm to integrate logistic regression and SVM based on re-selected features to explore whether the predictive performance could be improved.

One-way analysis of variance (ANOVA) and multivariate logistic regression were used to select independent predictive factors of clinical and radiological characteristics related to NSLN metastasis in the training set. In multivariate logistic regression, factors with $p < 0.05$ were considered as independent factors. The combined radiomics model (Model 8) was developed with the independent predictive factors and the best model from Models 1 to 7 by SVM classifier.

Comparison with the MSKCC model

As one of the most widely validated NSLN predictive models in the world, the MSKCC model was used to compare the predictive performance with the radiomics model. The pathological data of each patient in the external testing set were input to the MSKCC model (http://www.mskcc.org/nomograms) to obtain the probability of NSLN metastasis, and then the ROC curve of the MSKCC model was used to assess the predictive performance, and the AUCs of the radiomics model and the MSKCC model were compared in the external test set.

Statistical analysis

Statistical analysis was performed in Python (version 3.6), R software (version 3.4.1), and SPSS (version 26). The pathology results were used as the gold standard in judging whether NSLN had metastasis. Continuous variables were compared by t-test, while qualitative variables were analyzed by chi-square test or Fisher's exact test. Delong test was used to compare the difference between AUCs of radiomics model and MSKCC model in the external testing set. McNemar's test was used to compare the performance of radiomics model and MSKCC model. The "sklearn.feature_selection", "sklearn.linear_model", and " matplotlib.pyplot" function packages in Python were used to select radiomics features, while the "stats" package in R software was used for the selection of independent predictive factors. The "sklearn" and "pROC" packages in Python were used for radiomics model development and ROC analysis. A two-sided $p < 0.05$ was regarded as a statistically significant difference.

RESULTS

Clinical and radiological characteristics

About 58.6%, 58.3%, and 53.1% of patients had NSLN metastasis in the training, internal, and external testing sets, respectively. The clinical and radiological characteristics of patients in three sets are shown in Table 1. Significant difference in T stage ($p = 0.018$) was found between NSLN positive and NSLN negative in the training set.

Feature extraction and consistency assessment

A total of 1322 radiomics features were extracted from each ROI. Dice coefficients ranged from 0.83 to 0.95 in the same reader 1 and from 0.81 to 0.94 in two different readers, indicating good consistency in ROI segmentation. The ICCs ranged from 0.816 to 0.954 in the same reader 1 and from 0.773 to 0.935 in two different readers, indicated good reproducibility of radiomics feature extraction.

Predictive performance of radiomics models

A total of 6, 26, 26, 17, and 14 radiomics features were finally selected from I, P5, P10, *I* + P5, and *I* + P10 ROIs, respectively (Supplementary Table 1). Models 1–5 were developed with an AUC of 0.7004 (95% confidence interval [CI]: 0.5839–0.7372), 0.6558 (95% CI: 0.5564–0.7148), 0.6545 (95% CI: 0.5332–0.6937), 0.6781 (95% CI: 0.5535–0.7232), and 0.6933 (95% CI: 0.5552–0.7233), respectively, in the internal testing set by SVM classifier (Table 2). Then, using the radiomics features from intratumoral (I) ROI and intratumoral+peritumoral 10 mm (*I* + P10) ROI, a new radiomics model (Model 6) was developed by the

Table 1. Clinical and radiological characteristics in the training, internal and external testing sets

	Training set (n = 220)			Internal testing set (n = 96)			External testing set (n = 49)		
	NSLN positive (n = 129)	NSLN negative (n = 91)	P	NSLN positive (n = 56)	NSLN negative (n = 40)	P	NSLN positive (n = 26)	NSLN negative (n = 23)	P
Age, years (mean ± SD)	55.0 ± 9.9	53.7 ± 11.0	0.341	55.5 ± 10.0	55.9 ± 9.8	0.862	56.0 ± 11.3	56.2 ± 11.2	0.956
Diameter, cm (mean ± SD)	2.8 ± 1.0	2.5 ± 1.3	0.065	3.0 ± 1.3	2.2 ± 0.9	0.001*	2.4 ± 0.9	2.2 ± 0.7	0.242
ER			0.191			0.462			0.612
Negative	29 (22.5%)	14 (15.4%)		6 (10.7%)	2 (5.0%)		3 (11.5%)	1 (4.3%)	
Positive	100 (77.5%)	77 (84.6%)		50 (89.3%)	38 (95.0%)		23 (88.5%)	22 (95.7%)	
PR			0.381			0.186			1.000
Negative	32 (24.8%)	18 (19.8%)		8 (14.3%)	2 (5.0%)		3 (11.5%)	3 (13.0%)	
Positive	97 (75.2%)	73 (80.2%)		48 (85.7%)	38 (95.0%)		23 (88.5%)	20 (87.0%)	
HER2			0.273			0.853			1.000
Negative	100 (77.5%)	76 (83.5%)		47 (83.9%)	33 (82.5%)		23 (88.5%)	21 (91.3%)	
Positive	29 (22.5%)	15 (16.5%)		9 (16.1%)	7 (17.5%)		3 (11.5%)	2 (8.7%)	
Ki-67			0.535			0.494			0.731
Negative	20 (15.5%)	17 (18.7%)		7 (12.5%)	7 (17.5%)		6 (23.1%)	4 (17.4%)	
Positive	109 (84.5%)	74 (81.3%)		49 (87.5%)	33 (82.5%)		20 (76.9%)	19 (82.6%)	
Molecular Subtype			0.316			0.185			1.000
Luminal A	16 (12.4%)	14 (15.4%)		7 (12.5%)	7 (17.5%)		4 (15.4%)	3 (13.0%)	
Luminal B	85 (65.9%)	65 (71.4%)		43 (76.8%)	32 (80.0%)		20 (76.9%)	18 (78.3%)	
HER2 over expression	14 (10.9%)	4 (4.4%)		2 (3.6%)	1 (2.5%)		0 (0%)	1 (4.3%)	
Triple negative	14 (10.9%)	8 (8.8%)		4 (7.1%)	0 (0%)		2 (7.7%)	1 (4.3%)	
Lymphovascular invasion			0.729			0.791			0.648
Negative	101 (78.3%)	73 (80.2%)		46 (82.1%)	32 (80.0%)		13 (50.0%)	13 (56.5%)	
Positive	28 (31.7%)	18 (19.8%)		10 (17.9%)	8 (20.0%)		13 (50.0%)	10 (43.5%)	
Menstrual status			0.687			0.051			0.357
Menopausal	73 (56.6%)	49 (53.8%)		34 (60.7%)	28 (70.0%)		16 (61.5%)	17 (73.9%)	
Not menopausal	56 (43.4%)	42 (46.2%)		22 (39.3%)	12 (30.0%)		10 (38.5%)	6 (26.1%)	
T stage			0.018*			0.001*			0.254
Tis	1 (0.8%)	1 (1.1%)		0 (0%)	1 (2.5%)		0 (0%)	0 (0%)	
T1	29 (22.5%)	37 (40.7%)		12 (21.4%)	22 (55.0%)		8 (30.8%)	11 (47.8%)	
T2	93 (72.1%)	52 (57.1%)		40 (71.4%)	17 (42.5%)		18 (69.2%)	12 (52.2%)	

(Continued)

Table 1. (Continued)

	Training set (n = 220)			Internal testing set (n = 96)			External testing set (n = 49)		
	NSLN positive (n = 129)	NSLN negative (n = 91)	P	NSLN positive (n = 56)	NSLN negative (n = 40)	P	NSLN positive (n = 26)	NSLN negative (n = 23)	P
T3	6 (4.6%)	1 (1.1%)		4 (7.1%)	0 (0%)		0 (0%)	0 (0%)	
BPE			0.633			0.814			0.706
Minimal	25 (19.4%)	19 (20.9%)		13 (23.2%)	9 (22.5%)		4 (15.4%)	2 (8.7%)	
Mild	61 (47.3%)	49 (53.8%)		27 (48.2%)	16 (40.0%)		13 (50.0%)	15 (65.2%)	
Moderate	31 (24.0%)	16 (17.6%)		11 (19.6%)	10 (25.0%)		6 (23.1%)	5 (21.7%)	
Marked	12 (9.3%)	7 (7.7%)		5 (8.9%)	5 (12.5%)		3 (11.5%)	1 (4.3%)	
Density			0.437			0.464			0.907
Entirely fatty	28 (21.7%)	13 (14.3%)		12 (21.4%)	8 (20.0%)		3 (11.5%)	3 (13.0%)	
Scattered fibroglandular	39 (30.2%)	28 (30.8%)		23 (41.1%)	11 (27.5%)		9 (34.6%)	6 (26.1%)	
Heterogeneously dense	47 (36.4%)	41 (45.1%)		15 (26.8%)	16 (40.0%)	[td]	13 (50.0%)	12 (52.2%)	
Extremely dense	15 (11.6%)	9 (9.9%)		6 (10.7%)	5 (12.5%)		1 (3.8%)	2 (8.7%)	

BPE, background parenchymal enhancement; ER, estrogen receptor; HER2, human epidermal growth factor receptor 2; NSLN, non-sentinel lymph node; PR, progesterone receptor; SD, standard deviation.

SVM classifier, with an AUC of 0.8000 (95% CI: 0.6871–0.8266) in the internal testing set, higher than Model 1, which was based on intratumoral features alone (p = 0.0037) . The raw radiomics features of intratumoral (I) ROI and intratumoral+peritumoral 10 mm (I + P10) ROI were re-selected together, and 17 features were re-selected finally (Supplementary Table 2). Model 7, which was constructed by using the boosting algorithm to integrate logistic regression and SVM based on re-selected features, did not improve the predictive performance with Model 6, yielding an AUC of 0.7862 (95% CI: 0.6727–0.8165) in the internal testing set (Table 2).

In the training set, T-stage (p = 0.0024) was proven to be an independent factor in predicting NSLN metastasis. Model 8, which was developed with T stage and radiomics features from Model 6, did not improve the prediction performance, yielding an AUC of 0.7906 (95% CI: 0.6403–0.7891) in the internal testing set. Figure 3 displays the ROC curves of each radiomics model.

Model six achieved the highest predictive performance among all models in the internal testing set, containing six radiomics features from intratumoral ROI and 14 radiomics features from intratumoral+peritumoral 10-mm ROI with non-zero coefficients in LASSO logistic regression (Table 3, Figure 1). The accuracy, sensitivity, and specificity of Model six in the internal testing set were 0.7500, 0.8250, and 0.6964, respectively. The AUC, accuracy, sensitivity, and specificity of Model six in the external testing set were 0.7567 (95% CI: 0.6717–0.8678), 0.7551, 0.7826, and 0.7308, respectively (Figure 3C).

Comparison with the MSKCC model

The AUC of our proposed radiomics model (Model 6) was higher than that of the MSKCC model (AUC = 0.6681, 95% CI: 0.5148–0.8213) (p = 0.361) (Figure 3C). Meanwhile, Model six showed statistically significant higher sensitivity (0.7826 *vs* 0.4615, p = 0.003) than the MSKCC model. Accuracy in Model six was also higher than the MSKCC model (0.7551 *vs* 0.6327, p = 0.157), but was not statistically significant. The specificity of Model six was slightly lower than that of the MSKCC model (0.7308 *vs* 0.8261, p = 0.705) with no statistical significance.

DISCUSSION

The status of NSLN metastasis is related to the choice of treatment options for breast cancer patients with SLN metastasis. Preoperative assessment of NSLN metastasis status has important clinical significance.[28,29] Our multicenter study explored the potential ability of CEM-based radiomics in predicting NSLN metastasis. The radiomics model (Model 6), which was developed with features from intratumoral ROI and intratumoral+peritumoral 10 mm ROI, showed the best predictive performance, with AUCs of 0.8000 and 0.7567 in the internal and external testing sets, respectively.

Before the emergence of radiomics, many scholars had used clinical and pathological factors to predict NSLN metastasis. Gruber et al[30] established a logistic regression model to predict NLSN metastasis using clinical factors, yielding an AUC of 0.73 in the validation group. Reynders et al[28] used seven significant factors related to NSLN metastasis to establish a predictive model,

Table 2. Predictive performance of Models 1–8.

	Training set				Internal testing set				External testing set			
	AUC (95% CI)	Accuracy (95% CI)	Sensitivity (95% CI)	Specificity (95% CI)	AUC (95% CI)	Accuracy (95% CI)	Sensitivity (95% CI)	Specificity (95% CI)	AUC (95% CI)	Accuracy (95% CI)	Sensitivity (95% CI)	Specificity (95% CI)
Model 1 Intratumoral (I) ROI	0.7227 (0.6680–0.7791)	0.6545 (0.4761–0.8213)	0.6154 (0.5067–0.7142)	0.6822 (0.5939–0.7602)	0.7004 (0.5839–0.7372)	0.6354 (0.5283–0.7320)	0.7500 (0.5851–0.8684)	0.5536 (0.4155–0.6842)	NA	NA	NA	NA
Model 2 Peritumoral 5 mm (P5) ROI	0.8349 (0.7876–0.8820)	0.7682 (0.6976–0.8334)	0.7802 (0.6791–0.8583)	0.7597 (0.6747–0.8287)	0.6558 (0.5564–0.7148)	0.6250 (0.4967–0.7714)	0.7250 (0.5588–0.8492)	0.5536 (0.4162–0.6840)	NA	NA	NA	NA
Model 3 Peritumoral 10 mm (P10) ROI	0.8275 (0.7800–0.8741)	0.7818 (0.6803–0.8616)	0.8022 (0.7028–0.8764)	0.7674 (0.6830–0.8347)	0.6545 (0.5332–0.6937)	0.6146 (0.4715–0.7301)	0.5500 (0.3870–0.7035)	0.6607 (0.5206–0.7783)	NA	NA	NA	NA
Model 4 Intratumoral+Peritumoral 5 mm (*I* + P5) ROI	0.7582 (0.7058–0.8096)	0.7045 (0.6138–0.7702)	0.6484 (0.5401–0.7435)	0.7442 (0.6576–0.8152)	0.6781 (0.5535–0.7232)	0.6250 (0.4634–0.7352)	0.6750 (0.5079–0.8094)	0.5893 (0.4504–0.7159)	NA	NA	NA	NA
Model 5 Intratumoral + Peritumoral 10 mm (*I* + P10) ROI	0.7275 (0.6719–0.7846)	0.6545 (0.5709–0.7664)	0.6593 (0.5522–0.7531)	0.6512 (0.5620–0.7318)	0.6933 (0.5552–0.7233)	0.6458 (0.5769–0.8345)	0.6250 (0.4580–0.7658)	0.6607 (0.5205–0.7780)	NA	NA	NA	NA
Model 6 Features from I&(*I* + P10) ROIs	**0.7293 (0.6731–0.7888)**	**0.6682 (0.5934–0.7367)**	**0.3297 (0.2366–0.4368)**	**0.9070 (0.8403–0.9485)**	**0.8000 (0.6871–0.8266)**	**0.7500 (0.7052–0.8847)**	**0.8250 (0.6657–0.9211)**	**0.6964 (0.6034–0.7791)**	**0.7567 (0.6717–0.8678)**	**0.7551 (0.6113–0.8666)**	**0.7826 (0.7200–0.8728)**	**0.7308 (0.5306–0.7917)**
Model 7 Model 1 + Model 5	0.7252 (0.6704–0.7858)	0.6773 (0.6009–0.7515)	0.4835 (0.3776–0.5904)	0.8140 (0.7345–0.8750)	0.7862 (0.6727–0.8165)	0.7400 (0.6443–0.8760)	0.8000 (0.5572–0.8075)	0.6964 (0.5326–0.8086)	NA	NA	NA	NA
Model 8 Features from Model 6 + T stage	0.7358 (0.6827–0.7966)	0.6909 (0.6143–0.7632)	0.4176 (0.3170–0.5263)	0.8837 (0.8122–0.9309)	0.7906 (0.6403–0.7891)	0.7083 (0.6425–0.8781)	0.7750 (0.6108–0.8856)	0.6607 (0.5213–0.7781)	NA	NA	NA	NA
MSKCC model	NA	NA	NA	NA	NA	NA	[td]	NA	**0.6681 (0.5148–0.8213)**	**0.6327 (0.4829–0.7658)**	**0.4615 (0.3265–0.6438)**	**0.8261 (0.5758–0.8900)**

Note: AUC = area under the curve; CI = confidence interval; MSKCC = Memorial Sloan Kettering Cancer Center; NA = not available; ROI = region of interest.

Figure 3. (a, b) ROC curves of constructed radiomics models in the training and internal testing sets, respectively. (c) ROC curves of Model six and the MSKCC model tested by the external testing set.

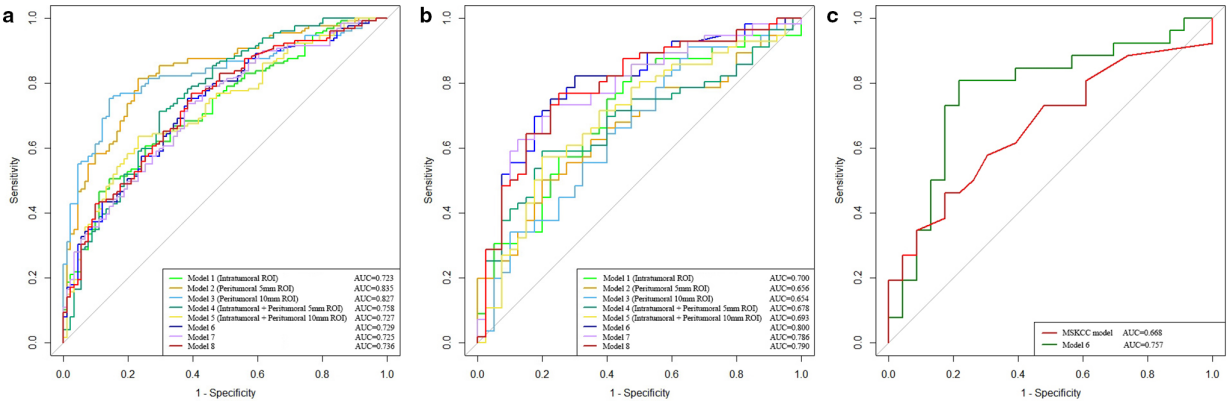

achieved the AUCs of 0.76 in the training set and 0.58 in one of the external sets, indicating that the generalization ability of the model needed to be further improved. Moreover, among the seven related factors, lymphovascular invasion and intraoperative positive SLN were obtained after the surgery, which might affect the use of the predictive model. In our study, the proposed radiomics model, which was established by radiomics features extracted from preoperative CEM images, had higher AUC than the well-known MSKCC model validated by external testing set (0.7567 *vs* 0.6681), indicating that the radiomics model had potential ability in predicting NSLN metastasis before surgery.

As an emerging discipline, radiomics, which combines traditional medical imaging with machine learning, can provide a stable and non-invasive approach to reflect the heterogeneity of tumors to a certain extent. More and more studies had confirmed that the peritumoral region could provide more information such as lymphocytic infiltration relating to SLN metastasis.[31] Liu et al[32] established a radiomics model based on intra- and peritumoral radiomics features extracted from dynamic contrast-enhanced MRI (DCE-MRI) to noninvasively predict SLN metastasis in breast cancer, yielding an AUC of 0.869 in the validation set, which was higher than that of the model using intratumoral

Table 3. LASSO coefficient profiles of the 20 features in Model 6

ROI	Radiomics Features	Modality	Coefficient
Intratumoral	wavelet-HHL_gldm_LargeDependenceEmphasis	Recombined	0.054211969
	wavelet-HLL_glszm_ZonePercentage	Low-energy	−0.027478837
	wavelet-HLL_glszm_ZonePercentage	Recombined	−0.002436579
	wavelet-HLL_gldm_SmallDependenceLowGrayLevelEmphasis	Low-energy	−0.012799902
	wavelet-LHH_glszm_LowGrayLevelZoneEmphasis	Low-energy	0.037350932
	wavelet-LHL_glrlm_ShortRunEmphasis	Recombined	−0.005482193
Intratumoral +Peritumoral 10 mm	wavelet-HHL_glszm_LargeAreaHighGrayLevelEmphasis	Low-energy	0.034885685
	wavelet-HHH_glrlm_GrayLevelVariance	Low-energy	0.024310428
	wavelet-HHH_glrlm_ShortRunEmphasis	Recombined	−0.016050074
	wavelet-HHH_glrlm_ShortRunLowGrayLevelEmphasis	Low-energy	−0.010330209
	wavelet-LHL_gldm_LargeDependenceHighGrayLevelEmphasis	Recombined	0.034539233
	wavelet-LLH_glszm_SizeZoneNonUniformity	Recombined	0.036595107
	wavelet-LLL_glszm_ZonePercentage	Low-energy	−0.029445573
	wavelet-HHH_glrlm_GrayLevelNonUniformityNormalized	Recombined	−0.019092896
	wavelet-HLL_firstorder_Kurtosis	Low-energy	0.034413406
	wavelet-LLH_glszm_SmallAreaEmphasis	Recombined	0.00273036
	wavelet-LLL_glrlm_RunLengthNonUniformity	Low-energy	−0.000597858
	wavelet-HHL_glszm_SizeZoneNonUniformityNormalized	Low-energy	−0.047975366
	wavelet-LLL_firstorder_InterquartileRange	Low-energy	0.014380025
	wavelet-HLL_glszm_SmallAreaEmphasis	Low-energy	0.003804684

radiomics features alone (AUC = 0.819). Similarly, Braman et al[33] used intra- and peri-tumoral radiomics features from DCE-MRI to predict pathological complete response to neoadjuvant chemotherapy of breast cancer, yielding an AUC of 0.740 in the independent testing set. In our study, Model 6, which used the radiomics features extracted from intratumoral and peritumoral regions, showed better predictive performance than the intratumoral model (AUC, 0.8000 *vs* 0.7004, $p = 0.0037$), indicating that the peritumoral features had certain significance in predicting NSLN metastasis.

Our research has several advantages. First, to our knowledge, using CEM-based radiomics to predict NSLN metastasis has not been previously reported. Second, considering that the peritumoral region of the breast cancer might provide additional information in predicting NSLN metastasis, we explored the predictive performance of radiomics based on different peritumoral regions (5 and 10 mm). The results showed that combining intratumoral and peritumoral regions could improve the predictive performance of the radiomics model. Third, an external testing set was used to verify the generalization ability of the proposed model, showing good predictive ability in NSLN metastasis.

Admittedly, this study has some limitations. First, although this study was one of the CEM-based radiomics studies with a relatively large number of patients, the number of patients enrolled in the external testing set was limited. A multicenter study with a larger sample size is warranted to prove the robustness of the proposed model. Second, as a feasibility study, the predictive performance of the radiomics model needs to be further improved for better clinical application. Deep learning method can automatically mine deep network features from images according to different tasks. Guo et al showed that ultrasound-based deep learning radiomics model had good predictive performance in predicting the SLN and NSLN metastasis of breast cancer.[34] In the future study, we will use larger sample data to explore whether CEM-based deep learning could improve predictive performance of NSLN metastasis. Third, although the types of CEM equipment at two centers are different, both are produced by the same company. Future studies will incorporate different CEM devices from more centers. Fourth, the segmentation of tumor ROIs was performed manually. Although Dice coefficients and ICCs showed good consistency and reproducibility, some studies found that semi-automatic and automatic segmentation methods had higher stability.[35,36] An automatic segmentation model will be trained to delineate the ROIs in the future study.

In conclusion, the radiomics model based on intratumoral and peritumoral regions of CEM images showed acceptable predictive performance in predicting NSLN metastasis of breast cancer patients, which can potentially benefit patients without NSLN metastasis by reducing unnecessary ALND. This study is a step toward precision medicine and personalized treatment for breast cancer patients. Further research on larger datasets with more centers is needed in the future.

ACKNOWLEDGMENT

Thanks to all participants in this study. Especially thanks, Ran Zhang, who is an employee of Huiying Medical Technology Co. Ltd, for providing technical support in this study.

FUNDING

This study was supported by the National Natural Science Foundation of China (82001775, 62176140), the Natural Science Foundation of Shandong Province (ZR2021MH120), and Special Foundation for Breast Disease Research of Shandong Medical Association (YXH2021ZX055).

REFERENCES

1. Siegel RL, Miller KD, Fuchs HE, Jemal A. Cancer statistics, 2021. *CA Cancer J Clin* 2021; **71**: 7–33. https://doi.org/10.3322/caac.21654
2. Kubikova E, Badidova J, Klein M, Beder I Jr, Benus R, Polak S, et al. Sentinel lymph node-historical background and current views on its significance in complex management of breast cancer patients. *Bratisl Lek Listy* 2019; **120**: 410–16. https://doi.org/10.4149/BLL_2019_066
3. Abass MO, Gismalla MDA, Alsheikh AA, Elhassan MMA. Axillary lymph node dissection for breast cancer: efficacy and complication in developing countries. *J Glob Oncol* 2018; **4**: 1–8. https://doi.org/10.1200/JGO.18.00080
4. Lucci A, McCall LM, Beitsch PD, Whitworth PW, Reintgen DS, Blumencranz PW, et al. Surgical complications associated with sentinel lymph node dissection (SLND) plus axillary lymph node dissection compared with SLND alone in the American College of surgeons Oncology Group trial Z0011. *J Clin Oncol* 2007; **25**: 3657–63. https://doi.org/10.1200/JCO.2006.07.4062
5. Sakorafas GH, Peros G, Cataliotti L. Sequelae following axillary lymph node dissection for breast cancer. *Expert Rev Anticancer Ther* 2006; **6**: 1629–38. https://doi.org/10.1586/14737140.6.11.1629
6. Qiao E, Yu X, Zhou L, Wang C, Yang C, Yu Y, et al. A prospective validation cohort study of a prediction model on non-sentinel lymph node involvement in early breast cancer. *Ann Surg Oncol* 2020; **27**: 1653–58. https://doi.org/10.1245/s10434-019-07980-x
7. Galimberti V, Cole BF, Zurrida S, Viale G, Luini A, Veronesi P, et al. Axillary dissection versus no axillary dissection in patients with sentinel-node micrometastases (IBCSG 23-01): a phase 3 randomised controlled trial. *Lancet Oncol* 2013; **14**: 297–305. https://doi.org/10.1016/S1470-2045(13)70035-4
8. Giuliano AE, Hunt KK, Ballman KV, Beitsch PD, Whitworth PW, Blumencranz PW, et al. Axillary dissection vs no axillary dissection in women with invasive breast cancer and sentinel node metastasis: a randomized clinical trial. *JAMA* 2011; **305**: 569–75. https://doi.org/10.1001/jama.2011.90
9. Hessman CJ, Naik AM, Kearney NM, Jensen AJ, Diggs BS, Troxell ML, et al. Comparative validation of online nomograms for predicting nonsentinel lymph node status in sentinel lymph node-positive breast cancer. *Arch Surg* 2011; **146**: 1035–40. https://doi.org/10.1001/archsurg.2011.201
10. Degnim AC, Reynolds C, Pantvaidya G, Zakaria S, Hoskin T, Barnes S, et al.

Nonsentinel node metastasis in breast cancer patients: assessment of an existing and a new predictive nomogram. *Am J Surg* 2005; **190**: 543–50. https://doi.org/10.1016/j.amjsurg.2005.06.008
11. Kocsis L, Svébis M, Boross G, Sinkó M, Maráz R, Rajtár M, et al. Use and limitations of a nomogram predicting the likelihood of non-sentinel node involvement after a positive sentinel node biopsy in breast cancer patients. *Am Surg* 2004; **70**: 1019–24. https://doi.org/10.1177/000313480407001119
12. Bi X, Wang Y, Li M, Chen P, Zhou Z, Liu Y, et al. Validation of the Memorial sloan kettering cancer center nomogram for predicting non-sentinel lymph node metastasis in sentinel lymph node-positive breast-cancer patients. *Onco Targets Ther* 2015; **8**: 487–93. https://doi.org/10.2147/OTT.S78903
13. Liu M, Wang S, Pan L, Yang D, Xie F, Liu P, et al. A new model for predicting non-sentinel lymph node status in Chinese sentinel lymph node positive breast cancer patients. *PLoS One* 2014; **9**(8): e104117. https://doi.org/10.1371/journal.pone.0104117
14. Lambin P, Rios-Velazquez E, Leijenaar R, Carvalho S, van Stiphout RGPM, Granton P, et al. Radiomics: extracting more information from medical images using advanced feature analysis. *Eur J Cancer* 2012; **48**: 441–46. https://doi.org/10.1016/j.ejca.2011.11.036
15. Gillies RJ, Kinahan PE, Hricak H. Radiomics: images are more than pictures, they are data. *Radiology* 2016; **278**: 563–77. https://doi.org/10.1148/radiol.2015151169
16. Mao N, Yin P, Wang Q, Liu M, Dong J, Zhang X, et al. Added value of radiomics on mammography for breast cancer diagnosis: a feasibility study. *Journal of the American College of Radiology* 2019; **16**: 485–91. https://doi.org/10.1016/j.jacr.2018.09.041
17. Mao N, Wang Q, Liu M, Dong J, Xiao C, Sun N, et al. Computerized image analysis to differentiate benign and malignant breast tumors on magnetic resonance diffusion weighted image. *Journal of Computer Assisted Tomography* 2019; **43**: 93–97. https://doi.org/10.1097/RCT.0000000000000793
18. Lin F, Wang Z, Zhang K, Yang P, Ma H, Shi Y, et al. Contrast-enhanced spectral mammography-based radiomics nomogram for identifying benign and malignant breast lesions of sub-1 cm. *Front Oncol* 2020; **10**: 573630. https://doi.org/10.3389/fonc.2020.573630
19. Wang Z, Lin F, Ma H, Shi Y, Dong J, Yang P, et al. Contrast-enhanced spectral mammography-based radiomics nomogram for the prediction of neoadjuvant chemotherapy-insensitive breast cancers. *Front Oncol* 2021; **11**: 605230. https://doi.org/10.3389/fonc.2021.605230
20. Sun Q, Lin X, Zhao Y, Li L, Yan K, Liang D, et al. Deep learning vs. radiomics for predicting axillary lymph node metastasis of breast cancer using ultrasound images: do ”t forget the peritumoral region. *Front Oncol* 2020; **10**: 53. https://doi.org/10.3389/fonc.2020.00053
21. Zhou J, Zhang Y, Chang K-T, Lee KE, Wang O, Li J, et al. Diagnosis of benign and malignant breast lesions on DCE-MRI by using radiomics and deep learning with consideration of peritumor tissue. *J Magn Reson Imaging* 2020; **51**: 798–809. https://doi.org/10.1002/jmri.26981
22. Li C, Song L, Yin J. Intratumoral and peritumoral radiomics based on functional parametric maps from breast DCE-MRI for prediction of HER-2 and Ki-67 status. *J Magn Reson Imaging* 2021; **54**: 703–14. https://doi.org/10.1002/jmri.27651
23. Lee-Felker SA, Tekchandani L, Thomas M, Gupta E, Andrews-Tang D, Roth A, et al. Newly diagnosed breast cancer: comparison of contrast-enhanced spectral mammography and breast MR imaging in the evaluation of extent of disease. *Radiology* 2017; **285**: 389–400. https://doi.org/10.1148/radiol.2017161592
24. Mao N, Yin P, Li Q, Wang Q, Liu M, Ma H, et al. Radiomics nomogram of contrast-enhanced spectral mammography for prediction of axillary lymph node metastasis in breast cancer: a multicenter study. *Eur Radiol* 2020; **30**: 6732–39. https://doi.org/10.1007/s00330-020-07016-z
25. Sorin V, Yagil Y, Shalmon A, Gotlieb M, Faermann R, Halshtok-Neiman O, et al. Background parenchymal enhancement at contrast-enhanced spectral mammography (CESM) as a breast cancer risk factor. *Acad Radiol* 2020; **27**: 1234–40. https://doi.org/10.1016/j.acra.2019.10.034
26. Lee CI, Chen LE, Elmore JG. Risk-based breast cancer screening: implications of breast density. *Med Clin North Am* 2017; **101**: 725–41. https://doi.org/10.1016/j.mcna.2017.03.005
27. Sogani J, Morris EA, Kaplan JB, D'Alessio D, Goldman D, Moskowitz CS, et al. Comparison of background parenchymal enhancement at contrast-enhanced spectral mammography and breast MR imaging. *Radiology* 2017; **282**: 63–73. https://doi.org/10.1148/radiol.2016160284
28. Reynders A, Brouckaert O, Smeets A, Laenen A, Yoshihara E, Persyn F, et al. Prediction of non-sentinel lymph node involvement in breast cancer patients with a positive sentinel lymph node. *Breast* 2014; **23**: 453–59. https://doi.org/10.1016/j.breast.2014.03.009
29. Liu D, Li X, Lan Y, Zhang L, Wu T, Cui H, et al. Models for predicting sentinel and non-sentinel lymph nodes based on pre-operative ultrasonic breast imaging to optimize axillary strategies. *Ultrasound Med Biol* 2021; **47**: 3101–10. https://doi.org/10.1016/j.ultrasmedbio.2021.06.014
30. Gruber I, Henzel M, Schönfisch B, Stäbler A, Taran F-A, Hahn M, et al. Prediction of non-sentinel lymph node metastases after positive sentinel lymph nodes using nomograms. *Anticancer Res* 2018; **38**: 4047–56. https://doi.org/10.21873/anticanres.12694
31. Takada K, Kashiwagi S, Asano Y, Goto W, Kouhashi R, Yabumoto A, et al. Prediction of lymph node metastasis by tumor-infiltrating lymphocytes in T1 breast cancer. *BMC Cancer* 2020; **20**(1): 598. https://doi.org/10.1186/s12885-020-07101-y
32. Liu C, Ding J, Spuhler K, Gao Y, Serrano Sosa M, Moriarty M, et al. Preoperative prediction of sentinel lymph node metastasis in breast cancer by radiomic signatures from dynamic contrast-enhanced MRI. *J Magn Reson Imaging* 2019; **49**: 131–40. https://doi.org/10.1002/jmri.26224
33. Braman NM, Etesami M, Prasanna P, Dubchuk C, Gilmore H, Tiwari P, et al. Intratumoral and peritumoral radiomics for the pretreatment prediction of pathological complete response to neoadjuvant chemotherapy based on breast DCE-MRI. *Breast Cancer Res* 2017; **19**: 57. https://doi.org/10.1186/s13058-017-0846-1
34. Guo X, Liu Z, Sun C, Zhang L, Wang Y, Li Z, et al. Deep learning radiomics of ultrasonography: identifying the risk of axillary non-sentinel lymph node involvement in primary breast cancer. *EBioMedicine* 2020; **60**: 103018. https://doi.org/10.1016/j.ebiom.2020.103018
35. Jung SC, Choi SH, Yeom JA, Kim J-H, Ryoo I, Kim SC, et al. Cerebral blood volume analysis in glioblastomas using dynamic susceptibility contrast-enhanced perfusion MRI: a comparison of manual and semiautomatic segmentation methods. *PLoS ONE* 2013; **8**: e69323. https://doi.org/10.1371/journal.pone.0069323
36. Parmar C, Rios Velazquez E, Leijenaar R, Jermoumi M, Carvalho S, Mak RH, et al. Robust radiomics feature quantification using semiautomatic volumetric segmentation. *PLoS One* 2014; **9**(7): e102107. https://doi.org/10.1371/journal.pone.0102107